Supporting Information

Al-Rekabi and Contera 10.1073/pnas.1719065115

SI Materials and Methods

Supported Lipid Bilayers. Supported lipid bilayers (SLBs) were obtained through the commonly used method, small unilamellar vesicle fusion (1). Circular mica surfaces (Ted Pella) were used as SLB substrates for the experiments. Initially, mica surfaces were mounted onto metal discs using high-vacuum silicone grease (Dow Corning). Freshly cleaved mica supports were initially lubricated with 100 mL of 20 mM NaCl. This was followed by placing 7 μL of small unilamellar vesicle suspension onto the mica and allowing them to settle at room temperature for 20 min. Next, the samples were rinsed several times with 20 mM NaCl to avoid unfused vesicles, but were always kept hydrated. The samples were then heated to 60 °C for 45 min. The SLB preparation process is shown in Fig. 1*B*.

AM–FM AFM. After slowly cooling down the sample, it was mounted onto the Asylum Research Cypher AFM (Oxford Instruments Asylum Research) and imaged. Using AM–FM mode, two separate excitation signals were combined to excite two cantilever resonances simultaneously. The principle of AM–FM operation in aqueous environment has been previously described (2–5). Briefly, the first resonance was monitored in standard tapping mode (AM mode), providing the topography through feedback on the first-resonance amplitude (Fig. 1*C*). Meanwhile, the cantilever was driven to oscillate at a second resonance, where the frequency was tracked by the controller (FM mode) (Fig. 1*C*). This implied that a stiffer sample will shift the oscillation of the higher normal mode to a higher frequency (6–8). Since AM–FM AFM involves the excitation of two cantilever eigenmodes (3, 4), we can therefore measure the deflection of cantilever as $z(t) = z_0 + A_2\cos(\omega_2 t - \varphi_2) + A_3\cos(\omega_3 t - \varphi_3) + O(\alpha)$, where z_0 is the mean deflection and $O(\alpha)$ contains higher-order terms, which are usually very small. The amplitude of the second eigenmode (A_2) is used to track the topography of the material, while the amplitude and phase of the third eigenmode are used to map both the conservative and dissipative components of the tip–sample interaction (3, 4, 9). In brief, the bimodal excitation and detection with FM mode of the AFM under aqueous conditions provides simultaneous information on both topography and local elastic modulus (storage) (3, 4). Furthermore, the signal of the lower frequency is used to establish the feedback mechanism as in regular FM AFM, while the higher frequency is sampled to provide the elastic modulus. Therefore, in AM–FM AFM quantitative information of materials are extracted from the projection of the continuous beam deflection over the cantilever eigenmodes. Applying both energy conservation and the virial theorem to the third eigenmode (free) gives two independent equations: $E_3^{\text{dissipated}} = -\int_0^T F_{\text{tip–sample}}(d)\cdot\dot{z}_3(t)dt = \pi k_3 A_3/Q_3(A_{0,3}\sin\varphi_3 - A_3)$ and $V_3^{\text{tip–sample}} = 1/T\int_0^T F_{\text{tip–sample}}(d)\cdot z_3(t)dt = -k_3A_{0,3}/2Q_3(A_3\cos\varphi_3)$, where $E^{\text{dissipated}}$ is the energy dissipated by the tip–sample forces, $V_{\text{tip–sample}}$ is the virial tip–sample forces, and $F_{\text{tip–sample}}$ is the tip–sample forces. The virial equation can be simplified using previous approximations (10) to express a relationship between the gradient of the interaction forces and phase shift of the third mode to give the following: $F'_{\text{tip–sample}}(d) \approx Ck_3A_{0,3}/A_3(z_c)Q_3\,[\cos\varphi_3(z_c)]$, where $A_{0,3}$, k_3, and Q_3 are the free amplitude, spring constant, and quality factor of the third eigenmode, respectively. There is a correction factor, C, that converges for high ratios ($A_{0,2}/A_{0,3}$), and finally, the relevant distances in the theory used for the tip–sample separation is $d = z + z_c = z_c - A_2 - A_3$. Using the Hertz contact model for a paraboloid indenter of radius R, the elasticity of the sample is related to the tip–sample stiffness by the relation $k_{\text{int}}(\delta) = 2E\sqrt{R\delta}$, where E is the elastic modulus (storage modulus) and δ is the indentation depth. Therefore, a relationship between φ_3 and E can be obtained where $F'_{\text{tip–sample}}(z_c) = 2E\sqrt{R\delta} = 2Er_c$, where r_c is the true contact radius, which has been derived in detail elsewhere (5). In the FM mode, the elastic moduli maps (E_{storage}) are determined by recording $A_3(x,y)$ and $\varphi_3(x,y)$, and hence we can determine those maps from the above equations, where $E = (1/2r_c)[k_3A_{0,3}/A_3(z_c)Q_3][\cos\varphi_3(z_c)]$. Consequently, as described elsewhere in detail (8, 11), a loss tangent map is obtained from the amplitude and phase signals in the AM mode. Since this technique is based on the Kelvin–Voigt viscoelastic model, we know that the loss tangent is equivalent to the ratio of the dissipated energy to stored energy ($\tan\delta = E_{\text{loss}}/E_{\text{storage}}$), allowing us to obtain the loss modulus ($E_{\text{loss}} = E_{\text{storage}}\tan\delta$). In this study, AM–FM AFM was used to estimate the E_{storage} and E_{loss} of DPPC:Chol (0–60%) lipid bilayers. We used OMCL-RC800PSA silicon nitride tips with a spring constant of 0.76 N/m (Olympus). Cantilevers were calibrated using the Sader method (12). The tip was brought in contact with the sample, and the drive frequency was carefully adjusted to the resonant frequency of the second normal mode of vibration of the cantilever ($f_2 \sim 150$ kHz) with a larger free amplitude at (~50–100 nm). Meanwhile, the cantilever was driven at a second resonance, characterized by higher frequency ($f_3 \sim 420$ kHz), corresponding to the third normal mode with much smaller amplitude (~0.5–2 nm). The third mode was adjusted to keep the phase at 90° on resonance. After the method was calibrated using a sample of known elastic modulus (DPPC), the tip was retracted, and the calibration sample was replaced by the sample of interest. When the tip-to-surface approach was completed, both resonances were tuned again. The drive set point of the second normal mode was 700–800 mV and that of the higher mode was 20 mV. A low A_3/A_0 ensured optimal tracking of the surface topography, which was important to obtain proper results in AM–FM AFM. All results in this work have been deposited in figshare (https://figshare.com/articles/PNAS_paper_zip/5894584).

Data Analysis. The images were rendered and postprocessed with the software IGOR PRO 6.2 (WaveMetrics). Postprocessing included cropping and flattening the images using the first, third, or histogram flatten order. In this study, E_{storage} and E_{loss} of mixtures of DPPC, DPPC:Chol (15%), DPPC:Chol (33%), and DPPC:Chol (60%) were obtained using IGOR. Histograms were plotted for the distribution of the moduli recorded for all pixels of the image. The histograms were fitted with Gaussian fits in Matlab (MathWorks), providing both the mean and SD (Table S1). All results presented in this work have been deposited in figshare (https://figshare.com/articles/PNAS_paper_zip/5894584).

1. Mingeot-Leclercq MP, Deleu M, Brasseur R, Dufrêne YF (2008) Atomic force microscopy of supported lipid bilayers. *Nat Protoc* 3:1654–1659.
2. Kocun M, Labuda A, Meinhold W, Revenko I, Proksch R (2017) Fast, high resolution, and wide modulus range nanomechanical mapping with bimodal tapping mode. *ACS Nano* 11:10097–10105.
3. Garcia R, Proksch R (2013) Nanomechanical mapping of soft matter by bimodal force microscopy. *Eur Polym J* 49:1897–1906.
4. Martinez-Martin D, Herruzo ET, Dietz C, Gomez-Herrero J, Garcia R (2011) Noninvasive protein structural flexibility mapping by bimodal dynamic force microscopy. *Phys Rev Lett* 106:198101.

5. Labuda A, Kocuń M, Meinhold W, Walters D, Proksch R (2016) Generalized Hertz model for bimodal nanomechanical mapping. *Beilstein J Nanotechnol* 7:970–982.
6. Guo S, et al. (2012) Multifrequency imaging in the intermittent contact mode of atomic force microscopy: Beyond phase imaging. *Small* 8:1264–1269.
7. Solares SD, Chawla G (2010) Triple-frequency intermittent contact atomic force microscopy characterization: Simultaneous topographical, phase, and frequency shift contrast in ambient air. *J Appl Phys* 108:054901.
8. Proksch R, Yablon DG (2012) Loss tangent imaging: Theory and simulations of repulsive-mode tapping atomic force microscopy. *Appl Phys Lett* 100:073106.
9. Lozano JR, Garcia R (2008) Theory of multifrequency atomic force microscopy. *Phys Rev Lett* 100:076102.
10. Kawai S, et al. (2009) Systematic achievement of improved atomic-scale contrast via bimodal dynamic force microscopy. *Phys Rev Lett* 103:220801.
11. Proksch R, et al. (2016) Practical loss tangent imaging with amplitude-modulated atomic force microscopy. *J Appl Phys* 119:134901.
12. Sader JE, Chon JWM, Mulvaney P (1999) Calibration of rectangular atomic force microscope cantilevers. *Rev Sci Instrum* 70:3967–3969.

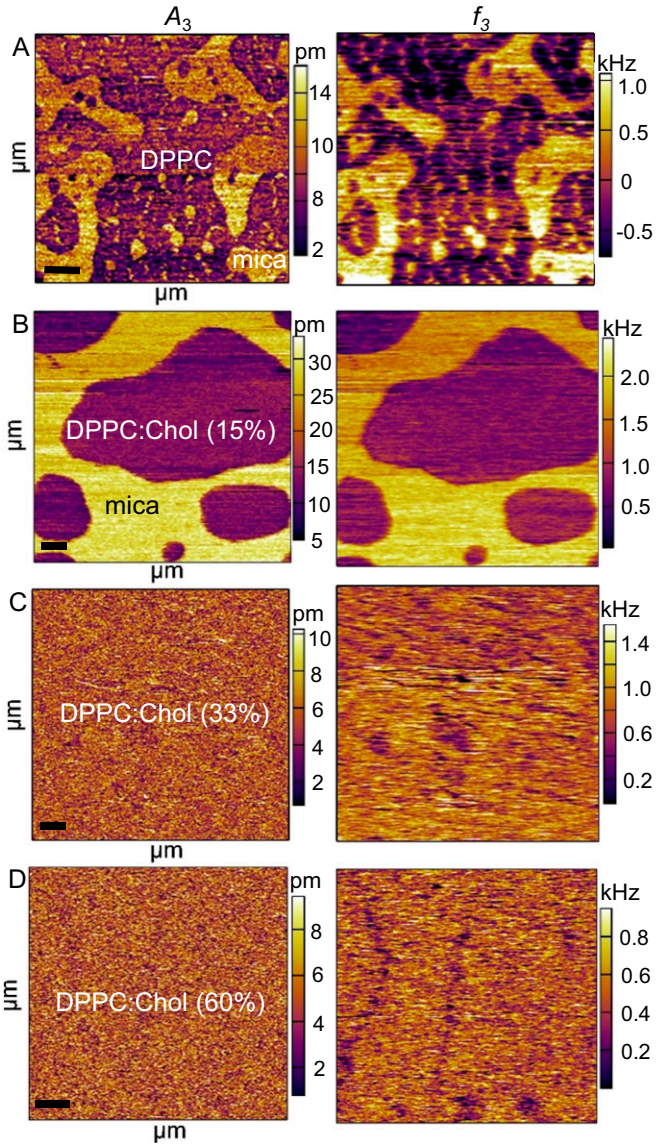

Fig. S1. The frequency modulation (FM) component of AM–FM AFM. The second resonance provides the amplitude (A_3) and frequency (f_3) information of DPPC:Chol with various molar fractions of Chol: (*A*) DPPC (0 mol %; scan size, 3.5 µm); (*B*) 15 mol % (scan size, 5.2 µm), which appears darker than the substrate, suggesting that the material is softer than the background; (*C*) both 33 mol % (scan size, 5.4 µm) and (*D*) 60 mol % (scan size, 3.8 µm) appear homogenous. [Scale bar: 500 nm (bottom left-hand corner).]

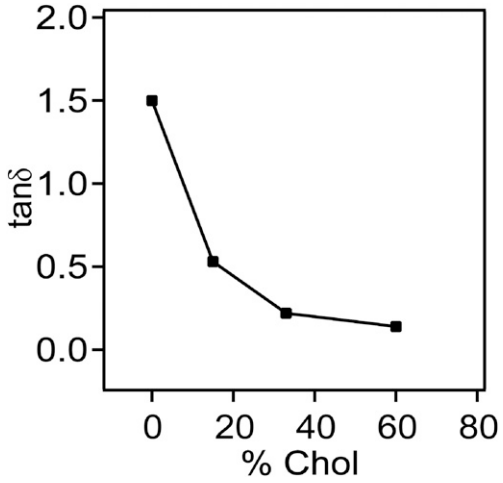

Fig. S2. Loss tangent values as function of molar fractions of Chol. The tanδ values for each respective mol percent of Chol in the DPPC:Chol model system.

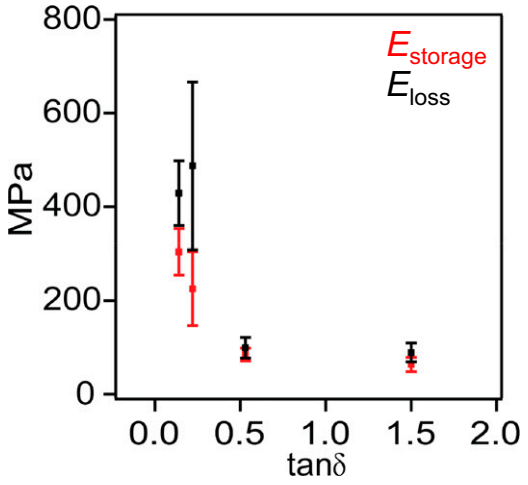

Fig. S3. Storage and loss moduli as a function of loss tangent values. The mean $E_{storage}$ (red) and E_{loss} (black) of the DPPC:Chol as function of the loss tangent values (tanδ). The error bars correspond to the SD.

Table S1. Storage and loss moduli of DPPC:Chol mixtures

DPPC:Chol mixtures	$E_{storage}$, MPa	E_{loss}, MPa
DPPC	63.3 ± 15.3	89.0 ± 20.0
DPPC:Chol (15%)	84.8 ± 13.5	99.2 ± 22.0
DPPC:Chol (33%)	225 ± 79.2	487 ± 179
DPPC:Chol (60%)	304 ± 49.4	429 ± 68.9